BIOCHEMISTRY
including biophysical chemistry & molecular biology

Article

pubs.acs.org/biochemistry

The Importance of Being Aromatic: π Interactions in Sodium Symporters

Xuan Jiang, Donald D. F. Loo, Bruce A. Hirayama, and Ernest M. Wright*

Department of Physiology, David Geffen School of Medicine at UCLA, Los Angeles, California 90095-1751, United States

ABSTRACT: In the LeuT family of sodium solute symporters, 13−17% of the residues in transmembrane domains are aromatic. The unique properties of aromatic amino acids allow them to play specialized roles in proteins, but their function in membrane transporters is underappreciated. Here we analyze the π bonding pattern in the LeuT (5TMIR) family and then describe the role of a triad of aromatic residues in sodium-dependent sugar cotransporters (SGLTs). In SLC5 symporters, three aromatic residues in TM6 (SGLT1 W289, Y290, and W291) are conserved in only those transporting sugars and inositols. We used biophysical analysis of mutants to discover their functional roles, which we have interpreted in terms of CH−π, π−π, and cation−π bonding. We discovered that (1) glucose binding involves CH−π stacking with Y290, (2) π T-stacking interactions between Y290 and W291 and H-bonding between Y290 and N78 (TM1) are essential to form the sodium and sugar binding sites, (3) the Na^+:sugar stoichiometry is determined by these residues, and (4) W289 may be important in stabilizing the structure through H-bonding to TM3. We also find that the WYW triad plays a role in Na^+ coordination at the Na1 site, possibly through cation−π interactions. Surprisingly, this Na^+ is not necessarily coupled to glucose translocation. Our analysis of π interactions in other LeuT proteins suggests that they also contribute to the structure and function in this whole family of transporters.

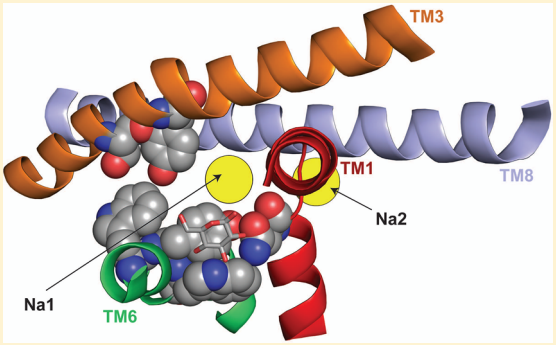

An advance in understanding symporters and antiporters was the crystallization of seven transporters from seven unrelated gene families. These proteins have a common architecture, the LeuT fold, consisting of an inverted repeat of five transmembrane helices (5TMIR) and a central occluded substrate binding site.[1−4] This, along with biophysical and biochemical evidence, indicates that members of the LeuT (5TMIR) structural family share a common alternating access transport mechanism.

The structures are rich in aromatic residues at the ends of helices and in the membrane interior; e.g., the aromatic residues are 15−17% of the total in the transmembrane (TM) core domain of vSGLT and LeuT (TM1−TM10)[1,2,5] (Figure 1). Aromatics can form two types of bonds: CH−π bonds between pairs of aromatic side chains in a T-stacking or an off-centered parallel orientation[6,7] and cation−π bonds that occur between basic and aromatic side chains.[8,9] In general, CH−π bonds in proteins occur in networks, and membrane proteins have a larger number of such networks than soluble proteins, suggesting a role in membrane protein stability.[10] There is computational evidence that there may be cooperativity between adjacent π−π and cation−π bonding sites.[11] Aromatic bonds in LeuT transporters form networks between TM helices of membrane proteins: in vSGLT the network engages TM6 with TM1, -2, -3, and -10 and TM2 with TM10 (Figure 1A), and in LeuT the network ties TM1 with TM2 and -6, TM3 with TM4, -8, and -10, TM4 with TM9, and TM5 with TM8 (Figure 1B).

Aromatic residues make unique associations with other residues; e.g., Y263 in vSGLT is part of a triad of aromatics on TM6 (Y262, Y263, and W264) conserved in glucose and inositol transporters but not the choline, iodide, multivitamin, or short chain fatty acid transporters (Figure 2).[12,13] Y263 forms a T-stacking π−π bond with W264, and Y262 is H-bonded to W134 on TM3. Whereas Y263 is the inner gate,[2,5] the outer gate is formed in part by a π−π bond between Y87 (TM2) and F424 (TM10). The triad is part of a larger network of interhelical aromatic bonds in vSGLT (Figure 1A).

There is a high degree of amino acid identity and similarity between vSGLT and hSGLT1 (32% identical and 69% similar), and key ligand binding and gate residues are conserved, including the aromatic triad [W289, Y290, and W291 (Figure 2 and ref 14)]. Unlike that by vSGLT, glucose transport by hSGLT1 is coupled to two Na^+ ions. Of the two Na^+ binding sites in hSGLT1, the putative Na2 site has been identified by homology with vSGLT and LeuT, but the identity of Na1 is unknown.[14] In LeuT, the Na1 site is located close to the leucine binding site.[1] In single cells, we are able to measure transport kinetics of wild-type and mutant human SGLT1 as a function of voltage ($K_{0.5}$ values and Hill coefficients for sugar and Na^+), the number of transporters in the plasma membrane, and the transport coupling ratio between Na^+ and sugar. Such assays are

Received: September 28, 2012
Revised: October 31, 2012
Published: November 1, 2012

dx.doi.org/10.1021/bi301329w | *Biochemistry* 2012, 51, 9480−9487

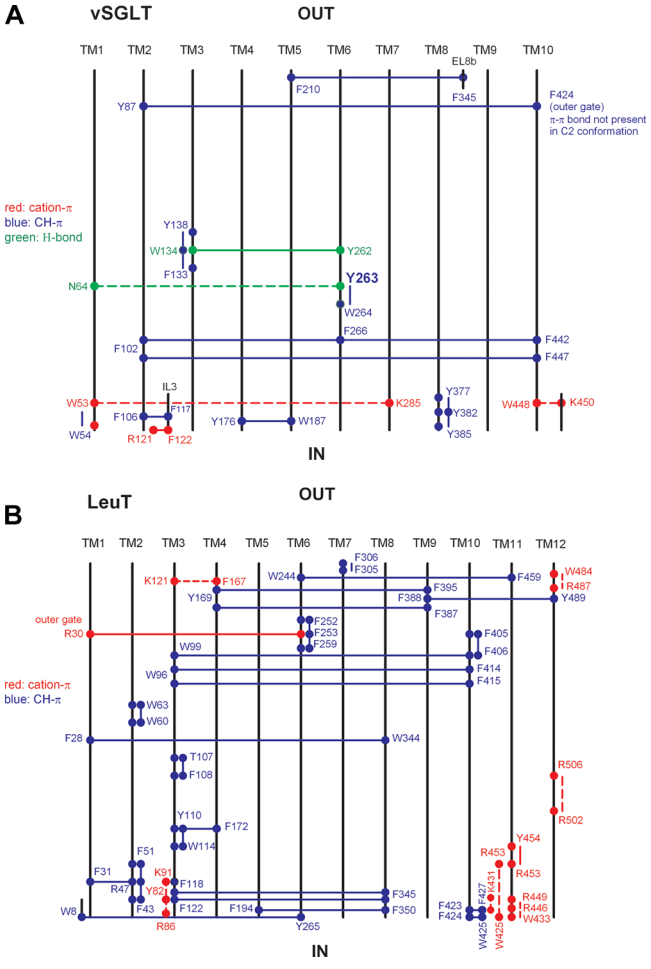

Figure 1. (A) Aromatic network in vSGLT. Potential aromatic interactions between TM in the core structure of vSGLT (TM1−TM10) were extracted from two conformations of vSGLT, inward facing occluded (PDB entry 3DH4) and inward facing open (PDB entry 2XQ2).[2,5] The linkages shown are those conserved among vSGLT and hSGLTs 1−6. The cation−π interactions were identified using CaPTURE, and the H-bond and CH−π interactions were identified by visual inspection of the structures. For cation−π bonds and H-bonds, the solid lines are interactions present in both 3DH4 and 2XQ2, whereas the dashed lines are interactions present in one but not both conformations. CH−π interactions are present in one or both conformations. (B) π interaction network in LeuT. The potential aromatic interactions between TM in the core structure of LeuT (TM1−TM10) were extracted from three conformations of LeuT, outward facing open (PDB entry 3TT1), outward facing occluded (PDB entry 2A65), and inward facing open (PDB entry 3TT3).[1,21] The cation−π interactions were identified using CaPTURE, and the CH−π interactions were identified by visual inspection of the structures. Solid lines are cation−π interactions present in all three conformations, and dashed lines are interactions not present in all three conformations. CH−π interactions are present in one or to two but not all three conformations.

not yet readily available for bacterial symporters. In this study, we have mutated in turn the conserved triad residues, W289, Y290, and W291, in hSGLT1 (Figure 2) and measured the kinetics of Na^+:sugar symport.

Our results show that the triad is a major determinant in Na^+ and sugar binding and transport by SGLTs, and that aromatic bonding (cation−π and CH −π) plays a central role in the function of hSGLT1 and other members of the LeuT structural family.

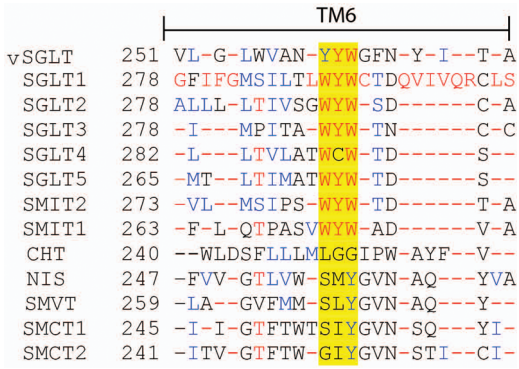

Figure 2. Sequence alignment of helix 6 of 12 human members of the SLC5 gene family. The amino acid sequence of helix 6 was from the crystal structure of *Vibrio parahemolyticus* vSGLT, and the human sequences were aligned using ClustalW (http://www.ebi.ac.uk) with manual adjustments. Strictly conserved and highly conserved residues are colored red and blue, respectively (single-letter code or red dashes). Gaps are indicated by black dashes. The location of the aromatic motif is highlighted in yellow. Abbreviations: SMIT, sodium myo-inositol; CHT, choline; SMVT, sodium multivitamin; SMCT, sodium monocarboxylic acid; NIS, sodium iodide symporter.[13]

MATERIALS AND METHODS

Oligonucleotide-Directed Mutagenesis. Mutations in hSGLT1 were introduced in plasmid hSGLT1-pBluescript using the QuickChange site-directed mutagenesis kit (Stratagene, La Jolla, CA). The mutagenic primers were designed taking into consideration the codon usage for humans to optimize protein expression. All constructs were verified by full gene sequencing.

Expression of hSGLT1 and Mutants in Oocytes. cRNA was synthesized and injected into *Xenopus laevis* oocytes as described in ref 14. Plasmid hSGLT1-pBluescript and its mutants were linearized with XbaI. Capped cRNAs were synthesized in vitro (T3 mMESSAGE mMACHINE kit, Applied Biosystems, Austin, TX). Stage V and VI *X. laevis* oocytes were injected with 50 ng of cRNA and incubated at 18 °C for 4−7 days in Barth's solution [88 mM NaCl, 10 mM HEPES-Tris, 2.4 mM $NaHCO_3$, 1.0 mM KCl, 0.8 mM $MgSO_4$, 0.4 mM $CaCl_2$, and 0.3 mM $Ca(NO_3)_2$ (pH 7.5)] supplemented with 5 μg/mL gentamicin, 100 μg/mL streptomycin, 100 units/mL penicillin, and 5.75 μg/mL ciprofloxacin. This protocol follows guidelines approved by the UCLA Chancellor's Committee on Animal Research.

Electrophysiological Experiments. Steady state kinetics was assessed using a two-electrode voltage clamp.[14] The oocytes were bathed in NaCl buffer [100 mM NaCl, 2 mM KCl, 1 mM $MgCl_2$, 1 mM $CaCl_2$, and 10 mM HEPES-Tris (pH 7.5)] with or without α-methyl-D-glucopyranoside (αMDG, a nonmetabolized sugar). A standard pulse protocol was used to determine the maximal pre-steady state charge movement Q_{max}, which is an index of the number of transporters expressed in the oocyte plasma membrane, and to measure the effect of membrane potential on transport. The membrane potential of oocytes was held at −50 mV (V_h) and stepped from 50 to −150 mV in 20 mV decrements for 100 ms before returning to V_h. All electrophysiological experiments were performed at 22 °C.

dx.doi.org/10.1021/bi301329w | *Biochemistry* 2012, 51, 9480−9487

Table 1. Summary of Wild-Type and Mutant Human SGLT1 Kinetics[a]

	$K_{0.5}^{\alpha MDG}$ (mM)	$K_{0.5}^{Na}$ (mM)	n^{Na}	I_{max} (nA)	SGLT density (×10^9)	"turnover number" (s^{-1})
SGLT1	0.6 ± 0.2	3 ± 0.1	1.5 ± 0.1	930 ± 232	14 ± 4	69 ± 4
W289C	nm	nm	nm	nm	5 ± 2	nm
W289Y	∼100	nm	nm	40 ± 14	nm	nm
Y290C	≫100	32 ± 4	1.6 ± 0.1	1315 ± 102	11 ± 1	>125 ± 5
Y290F	35 ± 10	20 ± 1	1.8 ± 0.2	1280 ± 361	15 ± 1	87 ± 19
W291C	>100	72 ± 29	1.9 ± 0.3	200 ± 48	9 ± 2	>19
W291F	4 ± 1	3 ± 1	1.5 ± 0.1	1269 ± 361	21 ± 7	61 ± 3

[a]Kinetic parameters are means ± the standard error from three to five oocytes from at least two donor frogs. $K_{0.5}^{\alpha MDG}$ and $K_{0.5}^{Na}$ are the half-saturation concentrations for αMDG and Na^+, respectively; n^{Na} is the Hill coefficient, and I_{max} is the maximal sugar-induced current. The number of transporters expressed in the plasma membrane is estimated from the maximal charge Q_{max}: 1 nC of Q_{max} is equivalent to 1 × 10^9 SGLT1 proteins expressed in the oocyte plasma membrane. The "turnover number" is obtained from the ratio $I_{max}^{-150\ mV}/Q_{max}$. All parameters were estimated at −150 mV, except n^{Na}, which was estimated at −50 mV. Note that $K_{0.5}^{\alpha MDG}$ is independent of membrane voltage between −50 and −150 mV while $K_{0.5}^{Na}$ is voltage insensitive for voltages more negative than −110 mV.[13]

Data were recorded using pClamp (Axon Instruments, Union City, CA).

Transporter Expression. The number of wild-type and mutant SGLT1 proteins expressed in the oocyte plasma membrane was estimated by measuring Q_{max} (maximal pre-steady state charge movement) in the presence of 100 mM Na buffer.[15] Q_{max} provides an index of the number of transporters: 1 nC of Q_{max} is equivalent to 1 × 10^9 SGLT1 proteins expressed in the plasma membrane.[15,16] Q_{max} was estimated by fitting the charge (Q) versus voltage data to a single Boltzmann function: $(Q - Q_{hyp})/Q_{max} = 1/\{1 + \exp[z\delta(V_m - V_{0.5})]F/RT\}$, where $Q_{max} = Q_{dep} - Q_{hyp}$, Q_{hyp} and Q_{dep} are the charges at the hyperpolarizing and depolarizing limits, respectively, V_m is the membrane potential, $V_{0.5}$ is the midpoint voltage, and $z\delta$ is the apparent valence of the voltage sensor.

The data in Table 1 show that the expression level all the 290 and 291 mutants was comparable to that of wild-type hSGLT1, >10 × 10^9 transporters in the plasma membrane (Q_{max} > 10 nC). The level of expression for W289C was approximately 25% of that for the wild type, 5 × 10^9 transporters in the membrane, but for W289F and W289Y, we were unable to detect Q values above the control oocytes, probably because of defects in trafficking of these proteins from the cytoplasm to the plasma membrane.

Measurement of Steady State Kinetics. Cotransport rates were obtained by subtracting the basal Na^+ current from the total current in the presence of sugar. The maximal sugar-induced current (I_{max}) and apparent sugar affinity ($K_{0.5}^{\alpha MDG}$) were then estimated by fitting the $I_{\alpha MDG}$ versus $[\alpha MDG]_o$ data to

$$I_{\alpha MDG} = I_{max}[\alpha MDG]_o/(K_{0.5}^{\alpha MDG} + [\alpha MDG]_o) \quad (1)$$

The apparent affinity for Na^+ ($K_{0.5}^{Na}$) was measured at different concentrations of Na^+ with a saturating concentration of αMDG. For the mutants with a high $K_{0.5}^{\alpha MDG}$, i.e., >100 mM, we estimated the kinetic constants in the presence of 100 mM αMDG. The external Na^+ concentration was varied by replacing NaCl with choline chloride. The sugar-induced current ($I_{\alpha MDG}$) was plotted as a function of external Na^+ concentration ($[Na]_o$) and fit to eq 2, where n is the Hill coefficient:

$$I_{\alpha MDG} = I_{max}([Na]_o)^n/[(K_{0.5}^{Na})^n + ([Na]_o)^n] \quad (2)$$

Stoichoimetry Determinations. The Na^+:sugar transport ratio was determined by measuring radiolabeled sugar or Na^+ uptake and sugar-induced inward charge simultaneously.[14,17,18] In brief, oocytes expressing the mutant or wild-type transporter were mounted in a microflow chamber in the two-electrode voltage clamp and continuously superfused with Na^+ buffer (in 100 mM NaCl, 2 mM KCl, 1 mM $MgCl_2$, 1 mM $CaCl_2$, and 10 mM HEPES) buffered with Tris to pH 7.5. The membrane potential of the oocyte was clamped at −50 or −90 mV. The experiment was initiated after a stable baseline current was reached by adding 1 mM αMDG containing [^{14}C]αMDG tracer (Perkin-Elmer). After the desired uptake interval, αMDG was removed and the oocyte washed until the baseline was re-established. The uptake of αMDG into each oocyte was determined by scintillation counting. Charge uptake was determined by integrating the current record over the time of the experiment and converting the inward charge from coulombs to p-equivalents of Na^+ using Faraday's constant. To confirm that inward charge was indeed equivalent to Na^+ uptake, parallel experiments were performed to simultaneously determine sugar-dependent inward charge and ^{22}Na uptakes using the same protocol that was used for charge and sugar uptakes. To optimize the specific activity of the isotope, these ^{22}Na measurements were taken at 10 mM NaCl (90 mM choline chloride replacing 90 mM NaCl) and αMDG concentrations varying between 10 and 50 mM to generate sufficient sugar-induced currents.

Statistics. Fits of data to equations were performed using either Sigmaplot 10 (SPSS, Inc., Chicago, IL) or Clampfit 10.1 (Axon Instruments). For data obtained on a single oocyte, the statistics are given by the estimates and the error of the fit. When data are from a population, the statistics are given by the means and the standard error of the means.

Structural Analysis. Aromatic interactions within the core domain (TM1−TM10) of transporter structures were extracted from the Protein Data Bank files, e.g., for vSGLT (2QX2 and 3DH4) and LeuT (2A65, 3TT1, and 3TT3). Energetically significant cation−π interactions were identified using CaPTURE available at http://capture.caltech.edu.[19] CH−π interactions and H-bonds were identified by visual inspection of the crystal structures in PyMol (DeLano Scientific, LLC).

RESULTS

Functional Analysis of the WYW Motif. *Steady State Kinetics.* Mutants were expressed in oocytes, and the kinetics of Na^+ and sugar transport was obtained using Na^+-dependent sugar-activated SGLT currents. The sugar-stimulated current is an inward Na^+ current that is directly proportional to sugar transport.[13,14]

dx.doi.org/10.1021/bi301329w | Biochemistry 2012, 51, 9480−9487

Sugar. An example of the electrophysiological assay in an oocyte expressing Y290F is shown in Figure 3. In NaCl buffer,

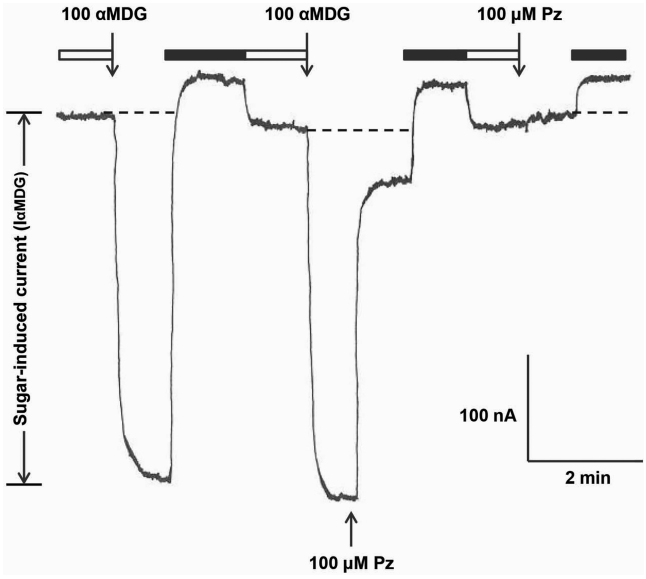

Figure 3. Na^+ current in a single oocyte treated with Y290F cRNA. The membrane potential of the oocyte was held at −50 mV. The horizontal dashed line indicates the baseline current in Na^+ medium in the absence of substrate. Addition of 100 mM αMDG to the extracellular Na^+ solution induced an inward current, which was inhibited by 100 μM Pz. The oocyte was washed in Na^+-free buffer (black box) before being returned to Na^+ buffer (white box).

addition of 100 mM αMDG rapidly produced an inward current because of the coupled inward transport of Na^+ and sugar. After washout of the substrates with Na^+-free buffer (choline Cl), the current was restored to the starting level in Na^+ buffer. The sugar-induced current ($I_{\alpha MDG}$) was obtained by subtracting the baseline current in Na^+ buffer from the current in the presence of αMDG. All Y290 and W291 mutants except Y290S exhibited sugar-induced currents. No sugar-induced currents were observed for Y289C even though the mutant was expressed in the plasma membrane (Table 1). This indicates that the sugar $K_{0.5}$ for Y289C is far in excess of 100 mM. On the other hand, 100 mM αMDG generated currents of 40 ± 14 nA (n = 4) and <10 nA for W289Y and W289F, respectively, but in these cases, the level of protein expression in the membrane was below the resolution of our method.

Apparent sugar affinities ($K_{0.5}^{\alpha MDG}$) and maximal sugar-induced currents (I_{max}) were estimated in 100 mM NaCl buffer at −150 mV by fitting $I_{\alpha MDG}$ versus $[\alpha MDG]_o$ to eq 1. The $K_{0.5}^{\alpha MDG}$ for wild-type SGLT1 was 0.4 mM, while substitution of the side chains of Y290 and W291 with cysteine (Y290C and W291C) resulted in a dramatic increase in $K_{0.5}^{\alpha MDG}$ to more than 100 mM (Table 1). Figure 4 shows single experiments with each mutant. For the wild type and W291F and Y290F mutants, currents saturated or were close to saturation at 100 mM sugar ($K_{0.5}$ values of 0.4, 3.7, and 23 mM, respectively). At 100 mM sugar, $I_{\alpha MDG}$ for Y290C and W291C was <50% of saturation, indicating that the αMDG $K_{0.5}$ for these mutants was greater than 100 mM. The data are summarized in Table 1. A phenylalanine side chain at position 290 partially restored sugar transport ($K_{0.5}$ values of 35 and >100 mM) showing the importance of both the aromatic side chain and the tyrosine OH group in Na^+/glucose cotransport by hSGLT1. At position

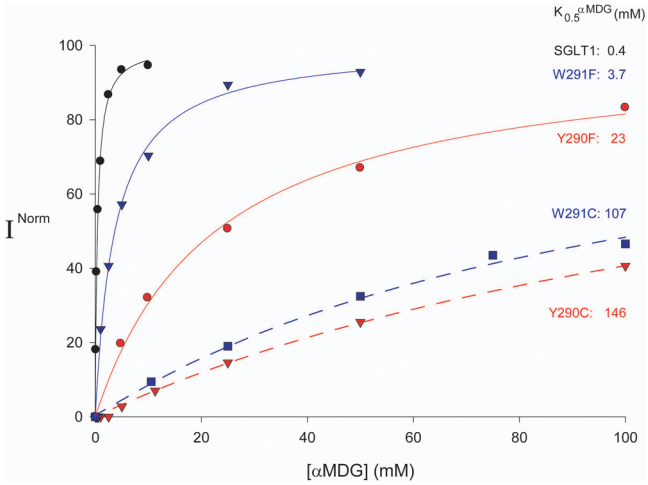

Figure 4. Steady state kinetics of the transport of αMDG by hSGLT1 and the mutants in 100 mM NaCl at −150 mV. The sugar-induced currents are normalized to the predicted I_{max} of each oocyte, and the normalized αMDG currents ($I_{\alpha MDG}/I_{max}$) are plotted as a function of $[\alpha MDG]_o$ and fit to eq 1. Similar results were obtained with at least three different batches of oocytes. The kinetic constants for each mutant are summarized in Table 1 from at least three batches of oocytes.

291, the tryptophan and phenylalanine side chains are almost equivalent in supporting sugar transport ($K_{0.5}^{\alpha MDG}$ values of 4 and 0.6 mM).

Turnover. The turnover rate, an estimate of the number of transport cycles each protein undergoes per second, was estimated from the ratio $I_{max}^{-150\ mV}/Q_{max}$.[15,16] For the phenylalanine mutants, the turnover number was similar to that of WT (~70 s^{-1}) (Table 1). However, only minimal rates can be estimated for W291C and Y290C, as the $K_{0.5}^{\alpha MDG}$ for these mutants is >100 mM at −150 mV. For Y290C, the turnover number was ≫100 s^{-1}, indicating either an increase in the actual rate of turnover or uncoupling of Na^+ and glucose transport.

Sodium. The apparent Na^+ affinity ($K_{0.5}^{Na}$) was measured at a saturating $[sugar]_o$. Sugar-induced currents ($I_{\alpha MDG}$) at −50 mV for the wild type and mutants were plotted as a function of external Na^+ concentration ($[Na]_o$) and fit to eq 2 (Figure 5). All position 290 and 291 mutants exhibited sigmoidal Na^+ activation kinetics with Hill coefficients between 1.5 and 2.2 (Figure 5 and Table 1). This shows that two Na^+ ions are required for activation of Na^+/glucose cotransport. Table 1 shows the $K_{0.5}^{Na}$ values for most mutants at −150 mV were 5−10 times higher than that of wild-type SGLT1 (15, 26, and 32 mM for Y290F, Y290C, and W291C, respectively, vs 3 mM for WT). The exception was W291F, for which the $K_{0.5}^{Na}$ was identical to that of WT (3 mM).

Transport Stoichiometry. The coupling between Na^+ and sugar transport for hSGLT1 is 2:1,[14,18,20] but mutations of outer gate residues increased coupling to as high as 6:1, i.e., uncoupled Na^+/glucose transport.[14] Here, we measured the coupling ratio of inner gate mutants W290F and W291F: it was impractical to measure the stoichiometry of W290C and W291C because of $K_{0.5}^{\alpha MDG}$ values of >100 mM. Figure 6 shows the plots of Na^+ (charge) versus αMDG uptake for individual oocytes expressing WT hSGLT1, W291F, and Y290F. For WT, the slope was 2.1 ± 0.1, whereas for both mutants, the slopes were close to 1:1. We confirmed that the

dx.doi.org/10.1021/bi301329w | *Biochemistry* 2012, 51, 9480−9487

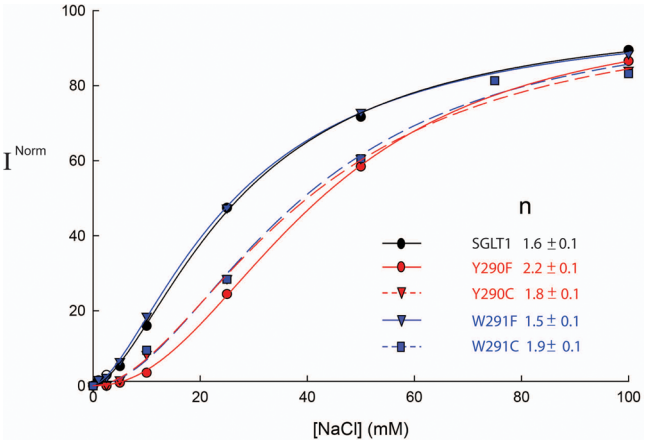

Figure 5. Na^+ activation of hSGLT1 αMDG currents at −50 mV. The sugar-induced current was measured in single cells at different Na^+ concentrations at a saturating sugar concentration for each mutant. The sugar-induced current was plotted as a function of external Na^+ concentration, and the data were fit to the Hill equation (eq 2), where n is the Hill coefficient and $K_{0.5}^{Na}$ is the apparent Na^+ affinity. For comparison, the sugar-induced current of each oocyte was normalized with I_{max}. Similar results were obtained in at least three different batches of oocytes (Table 1).

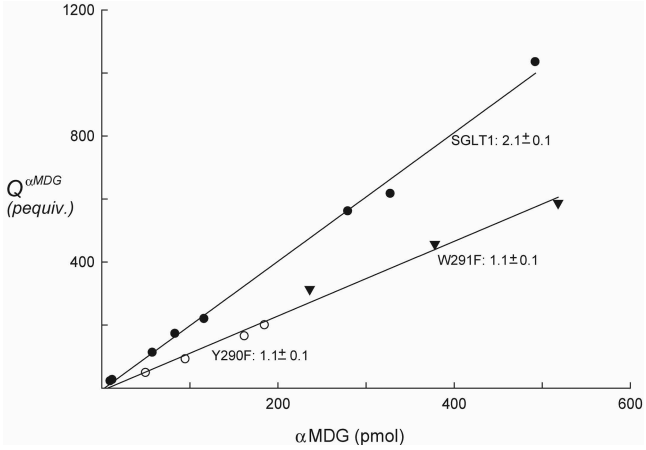

Figure 6. Determination of Na^+:glucose coupling ratios of SGLT1 and its mutants. αMDG uptake and inward charge were measured simultaneously over 5−10 min in each oocyte expressing WT SGLT1, Y290F, or W291F. Inward charge and sugar uptake were calculated as described in Materials and Methods. The slope is the Na^+:glucose coupling ratio. For each mutant, the experiments were repeated at least three times with different durations for sugar uptake. Note that for visual clarity only one line is shown for the mutants, but the slopes for each mutant are reported separately.

sugar-induced inward charge uptake was Na^+ uptake by measuring ^{22}Na uptake. The charge:^{22}Na ratios were 1.1 ± 0.1 (3), 0.7 ± 0.1 (3), and 1.2 ± 0.3 (3) for WT, W290F, and W291F, respectively.

DISCUSSION

Our understanding of the mechanism of sodium substrate cotransport improved with the advent of crystal structures of the LeuT structural family in several different conformations.[2,4,5,21−28] These structures confirm the alternate access transport model in which substrates bind to the protein on one side of the membrane and go through an intermediate state where the substrate is occluded from the aqueous media on both sides of the membrane before being released to the other side of the membrane. The substrate-binding sites, as well as the external and internal gates, have been identified. Furthermore, molecular dynamic simulations of vSGLT have provided insights into the structural basis of the underlying conformational changes; e.g., a plausible mechanism for the release of Na^+ and sugar from vSGLT into the cytoplasm is one in which the transition from outward to inward facing occluded conformations weakens binding of Na^+ to the Na2 site, resulting in disruption of the H-bond between inner gate residue Y263 and N64. Thus, a prediction is that Y263 adopts a new rotamer position to permit sugar exit.[5]

To understand the mechanism of symport, we have been using the human sodium/glucose transporter, hSGLT1, as a model system and have generated homology models of hSGLT1 based on vSGLT and other LeuT fold structures in different conformations. To infer the role of key residues, we related functional data from experiments with mutants. We have confirmed the importance of conserved residues forming the sugar binding site and the gates and provided structural insights into Na^+-induced external glucose binding and translocation to the internal aqueous release channel.[14] Here we focus on an aromatic motif, W289, Y290, and W291, conserved in the glucose and inositol transporters. Y290 corresponds to the inner gate residue in vSGLT (Y263) that is involved in both sugar binding and gating of the release of sugar to the cytoplasm.[5] Replacing the aromatic side chains of Y290 and W291 with cysteine dramatically reduced $K_{0.5}^{\alpha MDG}$ and $K_{0.5}^{Na}$ for Na^+/glucose cotransport and appeared to increase the turnover number.[14] Here, we have expanded the studies to include mutants of each of the three aromatic resides in the motif. The results show that W289, Y290, and W291 are part of an interactive network that forms the sugar binding site, the Na1 binding site, and in coupling of Na^+ and sugar cotransport.

Na^+ and Sugar Binding Functions of the Triad. The kinetics of hSGLT1 Y290C and Y291C[14] showed that the $K_{0.5}$ values for both sugar and Na^+ were dramatically decreased relative to that of WT (Table 1). The low affinity for sugar ($K_{0.5}^{\alpha MDG}$ > 100 mM) is compatible with the involvement of Y290 in sugar binding, but the loss of Na^+ affinity ($K_{0.5}^{Na}$ ~10-fold higher than that of WT) was surprising and suggested that residues 290 and 291 may be directly or indirectly involved in the binding of Na^+ at the Na1 site.

Replacement of Y290 with phenylalanine (Y290F) decreased $K_{0.5}^{\alpha MDG}$ compared to the value of Y290C, from ~170 to 35 mM, presumably by restoring the CH−π stacking interactions. Nevertheless, $K_{0.5}^{\alpha MDG}$ for Y290F is 50-fold higher than that of WT (0.6 mM). The tyrosine OH group is within H-bonding distance of N78 (TM1) (Figure 7), and $K_{0.5}^{\alpha MDG}$ for the N78A, -C, or -S mutant was 10-fold higher than in WT (ref 14 and unpublished data). Thus, H-bonding between N78 and Y290 appears to be crucial for the interaction of sugar and Na^+ with the transporter. We think that the H-bond between N78 and Y290 has two effects on $K_{0.5}^{\alpha MDG}$: positioning the aromatic ring for optimal interaction with sugar and the fact that the H-bond through the phenolic hydroxyl increases the electrostatic potential of the aromatic system, thereby increasing the strength of the interaction with the sugar.[29]

In contrast, W291F largely recovered the poor sugar and Na^+ affinities of the cysteine mutant [$K_{0.5}^{\alpha MDG}$ decreased from ~100 mM for W291C to 4.4 mM for W291F and $K_{0.5}^{Na}$ from 70 to 3 mM (Table 1)]. It is likely that the aromatic side chain at position 291 has a π−π interaction with Y290, stabilizing its

dx.doi.org/10.1021/bi301329w | Biochemistry 2012, 51, 9480−9487

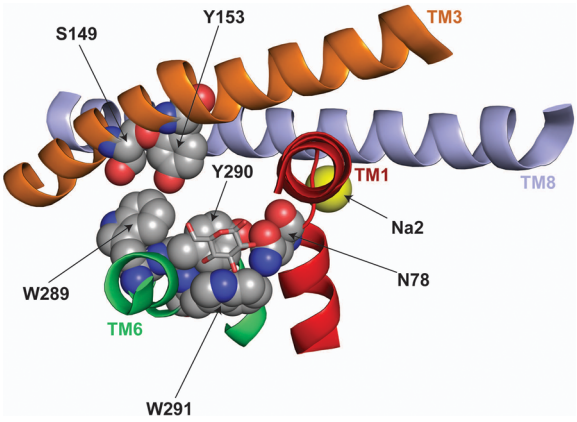

Figure 7. Homology model of the inward facing occluded structure of hSGLT1 based on the crystal structure of vSGLT. The reduced model shows only TM helices 1, 3, and 6 (LeuT numbering[3]), with the atoms of the side chains of residues N78, S149, Y153, W289, Y290, and W291 shown as spheres (black for C, red for O, and blue for N). Glucose is shown as a stick model and Na^+ in the Na2 site as a yellow sphere.

position, and W291 forms an H-bond with the 4-OH group of the sugar, or there is direct CH–π bonding between the sugar and W291 not evident in the X-ray structure. The loss of the phenolic hydroxyl also affected Na^+ affinity as the $K_{0.5}^{Na}$ for Y290F (20 mM) was 6-fold higher than for WT (3 mM) (Table 1). Neither Y290 nor W291 is within bonding distance of Na^+ at the Na2 site (Figure 7).

In Y290C and W291C, $K_{0.5}^{Na}$ increased from 3 to >30 mM, and for the W289 mutants, there was no apparent Na^+ binding. Because the putative Na2 site in vSGLT and hSGLT1 is >10 Å distant on the other face of TM1 (Figure 7), the effects are likely to be on the as yet unidentified Na1 binding site. The following possibilities exist. (1) Na^+ in the Na1 site might interact with W289, Y290, and/or W291 through cation–π interactions,[8] and/or (2) Na^+ directly interacts with bound glucose.[30,31] In LeuT, the Na1 binding site is close to the leucine binding site and the coordinating groups include the leucine COOH group and backbone carbonyls in the unwound region of TM1.[1] These results suggest that the Na1 site is close to the sugar-binding site in hSGLT1.

Na^+ and Sugar Coupling. The gate side chains are not simply barriers but play a role in the coupling of Na^+/sugar transport.[14] Mutation of each outer gate residue, L87C, F101C, and F453C, increased the Na^+:sugar stoichiometry above 2:1. In contrast, we found that the Na^+:sugar transport coupling ratios were reduced from 2:1 in WT to 1:1 in Y290F and W291F; i.e., only one sodium ion was transported with each sugar. However, Na^+ activation for all Y290 and W291 mutants was sigmoid [Hill coefficients in the range of 1.5–2.2 (Table 1)], indicating binding of two Na^+ ions is required for transport. An explanation for this difference between Na^+ activation and Na^+:glucose stoichiometry is that only one of the two Na^+ ions that bind to hSGLT1, probably the one at the Na2 site, is released into the cytoplasm with each sugar molecule, but Na^+ at the Na1 site returns to the external compartment.

Structural Model of Binding of Glucose to the Triad. Figure 7 is a model of hSGLT1 focused on the aromatic W289-Y290-W291 triad and related structural components in the inward facing occluded conformation.[14] Glucose is shown to overlie Y290. The fact that αMDG affinity was reduced by >2 orders of magnitude in the Y290C mutant (Table 1) indicates the close interaction between the pyranose ring and the aromatic ring as in sugar binding proteins.[32] It is now recognized that such stacking is mediated by π hydrogen bonds between the axial CH groups of the sugar and the aromatic side chain.[33] The OH group of Y290 is shown H-bonded to N78 (TM1) because mutation of each residue, Y290F and N78C, lowered the affinity for glucose by >1 order of magnitude (Table 1 and ref 14).

We further postulate that W289 (TM6) forms an H-bond with either S149 or Y153 (TM3): in both *Vibrio* SGLT structures, the homologous Y262 H-bonds with W134.[2] The effect of mutation W289C or W289F also indicates that W289 is important for sugar and/or Na^+ binding. W289C was well expressed in the oocyte plasma membrane (Table 1) but was insensitive to external Na^+ and sugar. Even for W289Y, there was poor sugar transport ($K_{0.5}$ ~ 100 mM). These results suggest an interaction between W289 and S149 or Y153 is critical for Na^+-coupled sugar transport possibly by stabilizing the nonhelical region of TM6. By analogy, in vSGLT the interaction between S365 (TM8) and E68 (TM1) has been proposed to stabilize the inward facing empty conformation.[5]

The interaction between Y263 and W264 in vSGLT[2,5] shows a typical edge-to-face geometry (T-stacking).[6,7,33] As shown in Table 1, replacement of the homologous W291 side chain in hSGLT1 with cysteine dramatically reduced the affinity for αMDG ($K_{0.5}$ > 100 mM), illustrating the importance of this aromatic interaction. These results point to the importance of the interactions between the TM6 aromatic triad and residues on TM1 and TM3 in maintaining the functional integrity of the transporter though a combination of classical and CH–π hydrogen bonds.

Broad Role of Aromatic Residues in LeuT Symporters. We have examined the role of the aromatic triad in hSGLT1. To assess the generality, we conducted an analysis of the aromatics in symporters. Figure 1 shows the network of aromatic interactions in vSGLT and LeuT. Ten intra-TM bonds and a comparable number (13) occur in LeuT. Given a binding energy of 1.5–3.3 kcal/mol per bond, these aromatic interactions are comparable to that of the network of classical H-bonds in other membrane proteins thought to be important in protein stability.[34]

Cation–π Bonds. The role of cation–π interactions has already been well recognized in binding of the ligand to ion channels, receptors, and transporters.[1,8,9,24,25] Here we identify significant cation–π interactions in symporters using CaPTURE.[19] For example, (1) in the open inward conformation of vSGLT (PDB entry 2QX2), there are interactions between K285 (TM7) and W53 (TM1) and between K450 and W448 (TM10) (2–3.6 kcal/mol) (Figure 1A), but these bonds do not exist in the inward occluded conformation (PDB entry 3DH4). (2) In LeuT, a cation–π bond between K121 and F167 (2.2–2.4 kcal/mol) ties the tops of TM3 and TM4 together in both the outward occluded and inward open conformations (PDB entries 2A65 and 3TT3, respectively) but not the outward open conformation (PDB entry 3TT1) (Figure 1B). (3) In all three conformations of LeuT [outward open (PDB entry 3TT1), outward occluded (PDB entry 2A65), and inward open (PDB entry 3TT3)], a bond occurs between R30 (TM1) and F253 (TM6) (2.6–4.1 kcal/mol). (4) Aromatic residues at the end of TM domains may form cation–π bonds with basic residues on interhelical loops; e.g.,

dx.doi.org/10.1021/bi301329w | *Biochemistry* 2012, 51, 9480–9487

in Mhp1 (PDB entry 2JLN), Y324 (TM8) interacts with K232 on the loop between TM6 and TM7. These observations suggest that cation−π bonds are involved in helix−helix packing and transitioning between conformations.

CH−π Bonds. Pairs of aromatic residues buried within the membrane core of vSGLT were identified where the phenyl rings are separated by <7.5 Å in T-stacking or off-centered parallel orientations (Figure 1A). Those in a T-stacking orientation include Y87 (TM2) and F424 (TM10), previously identified as outer gate residues; F102 (TM2) and F266 (TM6); F102 (TM2) and F447 (TM10); and Y263 and W264 (TM6) (Figure 1A). Those pairs in a parallel orientation include F266 (TM6) and F442 (TM10). In addition, a pair, W134 (TM3) and Y262 (TM6), are within H-bonding distance. This indicated that buried aromatic side chains are involved in defining the tertiary structure of vSGLT.

Ligand−Aromatic Interactions. Aromatic residues are essential elements in binding ligands. Binding of betaine to BetP involves cation−π interactions with three Trp residues in an aromatic box [Y189, W194, and W197 (PDB entry 2WIT[24,25])]. Binding of benzylhydantoin to Mhp1 has been modeled as $\pi-\pi$ stacking of hydantoin with Y117 and benzyl stacking with W220.[22] Finally, D-galactose in vSGLT stacks on the aromatic face of Y263,[2] presumably by CH−π bonding. In hSGLT1, the Y290C mutation reduces sugar transport affinity by >2 orders of magnitude. The magnitude of the difference in sugar affinity between Y290 (or Y290F) and Y290C is compatible with the loss of CH−π binding energy, 2−5 kcal/mol:[33] according to the Gibbs equation $\{K_1/K_2 = \exp[1 - \Delta(\Delta G)/RT]$, where K_1 and K_2 are the binding constants of WT and mutant proteins$\}$, the loss of 5 kcal/mol of binding energy would decrease the sugar binding constant by up to 300-fold.

In summary, our results highlight the importance of CH−π and cation−π hydrogen bonding in both ligand binding and the tertiary structure of sodium symporters in the LeuT structural family. Specifically, in hSGLT1, $\pi-\pi$ interaction (i) between outer gate residues F101 and F453 contributes to holding the sugar in the occluded conformation after binding, (ii) between sugar and Y290 determines the strength of sugar binding, and (iii) involving the WYW triad are intimately involved in the binding of Na to Na1, glucose binding, and release of sugar into the cytoplasm. More generally, we suggest that $\pi-\pi$ interactions are involved in determining the tertiary structure of LeuT transporters and transitions between conformational states.

AUTHOR INFORMATION

Corresponding Author

*Department of Physiology, David Geffen School of Medicine at UCLA, Los Angeles, CA 90095-1751. Telephone: (310) 825-6905. E-mail: ewright@medet.ucla.edu.

Funding

This work was supported by National Institute of Diabetes and Digestive and Kidney Diseases Grant DK19567.

Notes

The authors declare no competing financial interest.

ACKNOWLEDGMENTS

It is our pleasure to thank Drs. J. Abramson and A. Paz for stimulating discussions during this study and preparation of the manuscript.

ABBREVIATIONS

SSS, solute sodium symporters; LeuT, bacterial Na^+-coupled leucine transporter; vSGLT, Na^+/galactose symporter from *Vibrio parahemolyticus*; hSGLT1, human sodium/glucose cotransporter; αMDG, α-methyl-D-glucopyranoside; WT, wild type; 5TMIR, five-transmembrane inverted repeat; TM, transmembrane helix; $K_{0.5}^{Na}$, half-saturation concentration for Na^+; $K_{0.5}^{\alpha MDG}$, half-saturation concentration for αMDG; I_{max}, maximal sugar-induced current; $I_{\alpha MDG}$, sugar-induced current; PDB, Protein Data Bank.

REFERENCES

(1) Yamashita, A., Singh, S. K., Kawate, T., Jin, Y., and Gouaux, E. (2005) Crystal structure of a bacterial homologue of Na^+/Cl^--dependent neurotransmitter transporters. *Nature 437*, 215−223.

(2) Faham, S., Watanabe, A., Besserer, G. M., Cascio, D., Specht, A., Hirayama, B. A., Wright, E. M., and Abramson, J. (2008) The crystal structure of a sodium galactose transporter reveals mechanistic insights into Na^+/sugar symport. *Science 321*, 810−814.

(3) Abramson, J., and Wright, E. M. (2009) Structure and function of Na^+-symporters with inverted repeats. *Curr. Opin. Struct. Biol. 19*, 425−432.

(4) Krishnamurthy, H., Piscitelli, C. L., and Gouaux, E. (2009) Unlocking the molecular secrets of sodium-coupled transporters. *Nature 459*, 347−355.

(5) Watanabe, A., Choe, S., Chaptal, V., Rosenberg, J. M., Wright, E. M., Grabe, M., and Abramson, J. (2010) The mechanism of sodium and substrate release from the binding pocket of vSGLT. *Nature 468*, 988−991.

(6) Burley, S. K., and Petsko, G. A. (1985) Aromatic-aromatic interaction: A mechanism of protein structure stabilization. *Science 229*, 23−28.

(7) McGaughey, G. B., Gagne, M., and Rappe, A. K. (1998) π-Stacking interactions. Alive and well in proteins. *J. Biol. Chem. 273*, 15458−15463.

(8) Ma, J. C., and Dougherty, D. A. (1997) The Cation−π Interaction. *Chem. Rev. 97*, 1303−1324.

(9) Dougherty, D. A. (2007) Cation-π interactions involving aromatic amino acids. *J. Nutr. 137*, 1504S−1508S (discussion on pages 1516S−1517S).

(10) Chourasia, M., Sastry, G. M., and Sastry, G. N. (2011) Aromatic-Aromatic Interactions Database, A(2)ID: An analysis of aromatic π-networks in proteins. *Int. J. Biol. Macromol. 48*, 540−552.

(11) Vijay, D., and Sastry, G. N. (2010) The cooperativity of cation-π and π-π interactions. *Chem. Phys. Lett. 485*, 234−242.

(12) Turk, E., and Wright, E. M. (1997) Membrane topology motifs in the SGLT cotransporter family. *J. Membr. Biol. 159*, 1−20.

(13) Wright, E. M., Loo, D. D., and Hirayama, B. A. (2011) Biology of Human Sodium Glucose Transporters. *Physiol. Rev. 91*, 733−794.

(14) Sala-Rabanal, M., Hirayama, B. A., Loo, D. D., Chaptal, V., Abramson, J., and Wright, E. M. (2012) Bridging the gap between structure and kinetics of human SGLT1. *Am. J. Physiol. 302*, C1293−C1305.

(15) Loo, D. D., Hazama, A., Supplisson, S., Turk, E., and Wright, E. M. (1993) Relaxation kinetics of the Na^+/glucose cotransporter. *Proc. Natl. Acad. Sci. U.S.A. 90*, 5767−5771.

(16) Zampighi, G. A., Kreman, M., Boorer, K. J., Loo, D. D., Bezanilla, F., Chandy, G., Hall, J. E., and Wright, E. M. (1995) A method for determining the unitary functional capacity of cloned channels and transporters expressed in *Xenopus laevis* oocytes. *J. Membr. Biol. 148*, 65−78.

(17) Mackenzie, B., Loo, D. D., and Wright, E. M. (1998) Relationships between Na^+/glucose cotransporter (SGLT1) currents and fluxes. *J. Membr. Biol. 162*, 101−106.

(18) Quick, M., Loo, D. D., and Wright, E. M. (2001) Neutralization of a conserved amino acid residue in the human Na^+/glucose

transporter (hSGLT1) generates a glucose-gated H^+ channel. *J. Biol. Chem. 276*, 1728−1734.
(19) Gallivan, J. P., and Dougherty, D. A. (1999) Cation-π interactions in structural biology. *Proc. Natl. Acad. Sci. U.S.A. 96*, 9459−9464.
(20) Hummel, C. S., Lu, C., Loo, D. D., Hirayama, B. A., Voss, A. A., and Wright, E. M. (2011) Glucose transport by human renal Na^+/D-glucose cotransporters SGLT1 and SGLT2. *Am. J. Physiol. 300*, C14−C21.
(21) Krishnamurthy, H., and Gouaux, E. (2012) X-ray structures of LeuT in substrate-free outward-open and apo inward-open states. *Nature 481*, 469−474.
(22) Weyand, S., Shimamura, T., Yajima, S., Suzuki, S., Mirza, O., Krusong, K., Carpenter, E. P., Rutherford, N. G., Hadden, J. M., O'Reilly, J., Ma, P., Saidijam, M., Patching, S. G., Hope, R. J., Norbertczak, H. T., Roach, P. C., Iwata, S., Henderson, P. J., and Cameron, A. D. (2008) Structure and molecular mechanism of a nucleobase-cation-symport-1 family transporter. *Science 322*, 709−713.
(23) Shimamura, T., Weyand, S., Beckstein, O., Rutherford, N. G., Hadden, J. M., Sharples, D., Sansom, M. S., Iwata, S., Henderson, P. J., and Cameron, A. D. (2010) Molecular basis of alternating access membrane transport by the sodium-hydantoin transporter Mhp1. *Science 328*, 470−473.
(24) Ressl, S., Terwisscha van Scheltinga, A. C., Vonrhein, C., Ott, V., and Ziegler, C. (2009) Molecular basis of transport and regulation in the Na^+/betaine symporter BetP. *Nature 458*, 47−52.
(25) Perez, C., Koshy, C., Ressl, S., Nicklisch, S., Kramer, R., and Ziegler, C. (2011) Substrate specificity and ion coupling in the Na^+/betaine symporter BetP. *EMBO J. 30*, 1221−1229.
(26) Shaffer, P. L., Goehring, A., Shankaranarayanan, A., and Gouaux, E. (2009) Structure and mechanism of a Na^+-independent amino acid transporter. *Science 325*, 1010−1014.
(27) Fang, Y., Jayaram, H., Shane, T., Kolmakova-Partensky, L., Wu, F., Williams, C., Xiong, Y., and Miller, C. (2009) Structure of a prokaryotic virtual proton pump at 3.2 Å resolution. *Nature 460*, 1040−1043.
(28) Gao, X., Lu, F., Zhou, L., Dang, S., Sun, L., Li, X., Wang, J., and Shi, Y. (2009) Structure and mechanism of an amino acid antiporter. *Science 324*, 1565−1568.
(29) Mecozzi, S., West, A. P., Jr., and Dougherty, D. A. (1996) Cation-π interactions in aromatics of biological and medicinal interest: Electrostatic potential surfaces as a useful qualitative guide. *Proc. Natl. Acad. Sci. U.S.A. 93*, 10566−10571.
(30) Heaton, A. L., and Armentrout, P. B. (2008) Experimental and theoretical studies of sodium cation interactions with D-arabinose, xylose, glucose, and galactose. *J. Phys. Chem. A 112*, 10156−10167.
(31) Wincel, H. (2011) Thermochemistry of microhydration of sodiated and potassiated monosaccharides. *J. Am. Soc. Mass Spectrom. 22*, 1570−1576.
(32) Quiocho, F. A. (1989) Protein-carbohydrate interactions: Basis molecular features. *Pure Appl. Chem. 61*, 1293−1306.
(33) Nishio, M. (2011) The CH/π hydrogen bond in chemistry. Conformation, supramolecules, optical resolution and interactions involving carbohydrates. *Phys. Chem. Chem. Phys. 13*, 13873−13900.
(34) Bondar, A. N., and White, S. H. (2012) Hydrogen bond dynamics in membrane protein function. *Biochim. Biophys. Acta 1818*, 942−950.